Analyst

Cite this: *Analyst*, 2011, **136**, 1594

www.rsc.org/analyst

PAPER

A reliable and durable approach for real-time determination of cellular superoxide anion based on biomimetic superoxide dismutase stabilized by a zeolite

Jinqing Zhou, Yongping Luo, Anwei Zhu, Yan Liu, Zhirong Zhu and Yang Tian*

Received 6th September 2010, Accepted 28th January 2011
DOI: 10.1039/c0an00690d

This paper demonstrates a reliable and durable method for *in situ* real-time determination of $O_2^{\bullet -}$ based on direct electron transfer of $Mn_3(PO_4)_2$, which acts as a superoxide dismutase (SOD). Mn^{2+} is ion-exchanged into zeolite–ZSM-5 microstructures, and further coated with poly(diallyldimethylammonium chloride) (PDDA). Direct electron transfer of Mn^{2+} is greatly facilitated by zeolite microstructures with the formal potential of 561 ± 6 mV *vs.* Ag|AgCl, which is just located between thermodynamic potentials of $O_2^{\bullet -}/O_2$ and $O_2^{\bullet -}/H_2O_2$. The biomimetic catalytic activity of $Mn_3(PO_4)_2$, together with the enhanced electron transfer of Mn^{2+} obtained at the zeolite electrode has provided a platform for determination of $O_2^{\bullet -}$ with high selectivity, wide linear range, low detection limit, and quick response. On the other hand, the present Mn^{2+}-ZSM/PDDA electrode shows relatively long-term stability, good reproducibility, and biocompatibility, which opens up a way to adhering cells directly onto the film surface for *in situ* monitoring of cellular species. As a sequence, the remarkable analytical performance of the present $O_2^{\bullet -}$ biosensor, combined with the characteristics of the Mn^{2+}-ZSM/PDDA electrode surface has established a novel approach for real-time determination of $O_2^{\bullet -}$ released from living cells.

Introduction

Superoxide anion ($O_2^{\bullet -}$) is the primary species of reactive oxygen species (ROS), which defends against viral or bacterial attack, as well as destroys organisms if it exceeds the normal level.[1–4] Superoxide anion is believed to be closely implicated in a number of biological phenomena, such as aging, neurodegeneration, diabetes, cancers, and so on.[5] Therefore, local determination of $O_2^{\bullet -}$ could improve our understanding on the pathology and physiology processes involved with $O_2^{\bullet -}$.

Over the past decades, a large amount of methods have been developed for $O_2^{\bullet -}$ detection, including spectrophotometry, chemiluminescence, ESR spin trapping, and electrochemical methods.[6–9] Electrochemical approaches are of particular interest because of their simplicity, selectivity, low instrumental cost, and capability in real-time, and even *in vivo* detection. There have been many papers concerned with the electrochemical measurement of $O_2^{\bullet -}$, typically based on the incorporation of enzymes onto electrodes.[10–13] The two main enzymes employed in the construction of $O_2^{\bullet -}$ biosensor are cytochrome (cyt *c*) and superoxide dismutase (SOD). SOD-based $O_2^{\bullet -}$ biosensors have paved an elegant way for determination of $O_2^{\bullet -}$ with high selectivity, low detection limit, and good sensitivity.[14–17] However, these kinds of biosensors based on biomolecules are easy to be denatured or metabolized in the long-term real sample detection although they possess high selectivity and sensitivity.

Recently, we have reported a facile and effective strategy for analysis of $O_2^{\bullet -}$, through direct electron transfer of a biomimetic SOD—manganese(II) phosphate ($Mn_3(PO_4)_2$) at highly conductive TiO_2 nanoneedles.[18] In order to further improve the stability and durability of $O_2^{\bullet -}$ biosensor, herein a zeolite—ZSM-5 with rich acidic sites, which can provide a high cation-exchange capacity, is employed to stabilize the biomimetic SOD, and PDAA is further coated onto zeolite to confine Mn^{2+}-exchanged zeolite on the electrode substrate. As expected, the PDDA-coated Mn^{2+}-exchanged zeolite surface (denoted as Mn^{2+}-ZSM/PDDA) exhibits relatively long-term stability, durability, and biocompatibility. These properties provide a reliable platform to adhere living cells directly on the electrode surface for real-time assaying of cellular species. On the other hand, $O_2^{\bullet -}$ biosensor based on direct electron transfer of $Mn_3(PO_4)_2$ shows remarkable analytical performance, including high selectivity, broad detection linear range, quick response, and so on. Thus, the present work has established a reliable and durable approach for *in situ* monitoring of $O_2^{\bullet -}$ released from living cells.

Department of Chemistry, Tongji University, Siping Rode 1239, Shanghai, 200092, China. E-mail: yangtian@mail.tongji.edu.cn; Fax: +86 21 65981097; Tel: +86 21 65987075

Experimental section

Chemicals and reagents

Potassium hyperoxide (KO_2) was obtained from Sigma and used without further purification. Dimethyl sulfoxide (DMSO), $MnSO_4$, H_2O_2 and K_3PO_4 were obtained from Sinopharm Chemical Reagent Co., Ltd. A stock solution of KO_2 was prepared by adding KO_2 to DMSO, and then sonicating the solution for 5 min. Uric acid (UA), dopamine (DA), ascorbic acid (AA), L-cysteine (Cys) and sodium molybdenum oxide dihydrate were purchased from Alfa Aesar. Poly-(diallyldimethylammonium chloride) (PDDA, M_w < 200 000) was obtained from Aldrich. Peroxynitrite ($ONOO^-$) was purchased from R&D Systems. 2,2-Azobis(2-amidinopropane)-dihydrochloride (AAPH) was purchased from Adamas-beta. $OH^{\bullet}$ was generated in 10 μM H_2O_2 catalyzed by Fe^{2+}. $ONOO^-$ (10 μM) was generated by diluting commercially available peroxynitrite solution with a strongly basic solution (0.1 M NaOH). $^1O_2$ was generated as a product of the disproportionation of 20 μM H_2O_2 catalyzed by sodium molybdenum oxide dehydrate. $ROO^{\bullet}$ was produced by thermolysis of 10 μM AAPH in air-saturated aqueous solution at 310 K. Indium tin oxide (ITO)-coated glass plates were obtained from Shenzhen Nanbo Display Technology Co. Ltd. (Shenzhen, China). All solutions were prepared with deionized water purified with a Milli-Q system.

Characterization and measurements

XRD data were obtained by a D/max2550VB3+/PC X-ray diffractometer using Cu (40 KV, 100 mA). Scanning electron microscopy (SEM) was carried out using a Hitachi S-4800. Atomic absorption spectroscopy was determined by an Agilent AA 3510. Electrochemical experiments were performed at room temperature by using a three-electrode setup, with a KCl saturated Ag|AgCl reference electrode and a platinum wire counter electrode. All electrochemical measurements were recorded by using a CHI 660 electrochemical working station from CH Instruments (Chenhua, Shanghai).

Preparation of zeolite and zeolite-modified electrodes

ZSM-5 zeolite of Si/Al = 15 was synthesized according to the reported procedure.[19] The as-synthesized ZSM-5 was exchanged with 0.01 M NH_4NO_3 solution at 363 K. Then the NH_4-form ZSM-5 was transferred to H-form ZSM-5 by calcination at a temperature of 823 K for 2 h.[20] Manganese cations were introduced into the H-form zeolites by the conventional cation-exchange process. Typically, 0.2 g ZSM-5 was immersed in 50 mL 0.02 M aqueous solution of manganese sulfate at a pH = 4.3. The mixture was kept at 353 K for 24 h. The residue was filtered and washed with hot distilled water, until the obtained products were free from ions and dried in air at room temperature. In order to determine the percentage of Mn^{2+} present in Mn^{2+}-ZSM zeolite, 0.02 g Mn^{2+}-ZSM zeolite was dissolved in 40% HF, then diluted to 100 mL with water. The concentration of Mn^{2+} was measured by atomic absorption spectroscopy. According to atomic absorption determination, the percentage of Mn^{2+} is 0.75 wt%. The Mn^{2+}-exchanged zeolite thus formed was denoted as Mn^{2+}-ZSM, while Mn^{2+} just mixed with zeolite was denoted as Mn^{2+}/ZSM. The zeolite-modified electrode was prepared by the following step: firstly, the ITO was in turn cleaned in the soapy water, neat ethanol, 1 M NaOH, and water. The electrode was then coated with Mn^{2+}-ZSM or Mn^{2+}/ZSM sol by a spin coating technique, after that one-layer PDDA was deposited on the zeolite and was allowed to dry under ambient condition to obtain Mn^{2+}-ZSM/PDDA electrode or Mn^{2+}/ZSM/PDDA electrode.

Results and discussion

Characterization of Mn^{2+}-ZSM surface

The SEM image of ZSM-5 is shown in the inset of Fig. 1. From this image, we can see that the size of zeolite crystal with an almost cubic shape is ~0.1 μm. After ion exchange, the same shape and size of zeolite crystal have been preserved. Fig. 1 illustrates the XRD spectra of ZSM-5 microcrystals and Mn^{2+}-ZSM microcrystals. After loading the Mn^{2+}, the decrease of the low-angle peak intensity is observed (curve b) due to the influence of the pore filling, indicating Mn^{2+} is exchanged into the zeolite.

Electrochemical Behavior of Mn^{2+}-ZSM/PDDA electrode

As shown in Fig. 2, one couple of well-defined redox peaks was observed at the as-prepared Mn^{2+}-ZSM/PDDA electrode surface in K_3PO_4 solution (curve c), while no electrochemical response was obtained at a bare zeolite (curve a) or a PDDA-coated zeolite surface (curve b). These observations indicate that the anodic and cathodic peaks are attributed to the redox reaction of Mn^{2+} ion-exchanged into the zeolite structures. The formal potential ($E^{0\prime}$) of Mn^{2+} after ion-exchanged with zeolite was estimated to be 561 ± 6 mV *versus* Ag|AgCl (in saturated KCl). For the comparison, the cyclic voltammogram (CV) for Mn^{2+}/ZSM/PDDA surface in the same solution was also given in Fig. 2d. One pair of redox peaks was also obtained at this surface with an

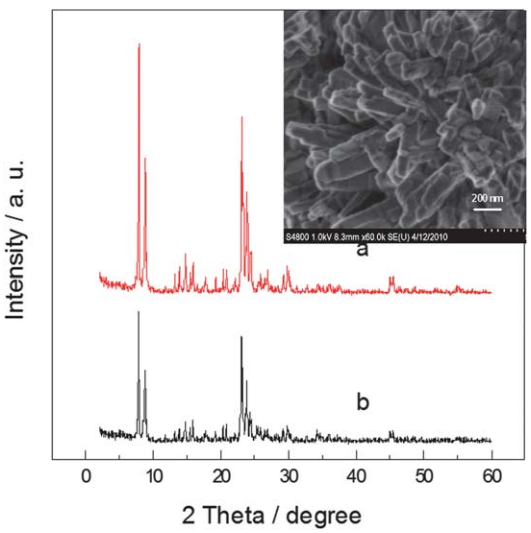

Fig. 1 XRD patterns for ZSM-5 (a) and Mn^{2+} ion-exchanged with zeolite (Mn^{2+}-ZSM, (b)). Inset: SEM image of ZSM-5.

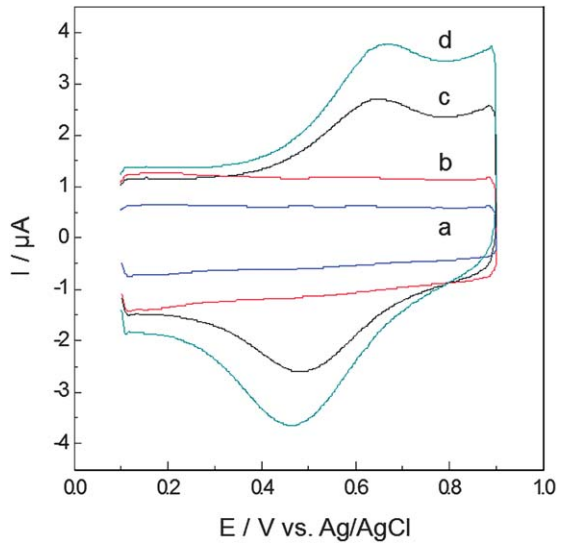

Fig. 2 Cyclic voltammograms (CVs) obtained at (a) ZSM electrode, (b) ZSM/PDDA electrode, (c) Mn^{2+}-ZSM/PDDA electrode, and (d) Mn^{2+}/ZSM/PDDA electrode in 50 mM K_3PO_4 solution (pH 7.0). Potential scan rate: 100 mV s^{-1}.

$E^{0\prime}$ of 557 ± 6 mV *versus* Ag|AgCl, which is similar to that obtained at Mn^{2+}-ZSM/PDDA surface.

CVs obtained at Mn^{2+}-ZSM/PDDA and Mn^{2+}/ZSM/PDDA electrodes with different potential scan rates are also obtained. The corresponding relationship between peak currents and scan rate (v) or square root of scan rate ($v^{1/2}$) was plotted in Fig. 3. From these plots, we can see that peak currents obtained at Mn^{2+}-ZSM/PDDA surface is linear with v, while those obtained at Mn^{2+}/ZSM/PDDA surface shows a clear linearity with $v^{1/2}$. This result suggests that Mn^{2+} exchanged into zeolite is strongly immobilized in intracrystalline surface of zeolite structures, thus the redox reaction of Mn^{2+} in zeolite microstructures is surface-confined process. However, the redox process for Mn^{2+} just mixed with zeolite and adsorbed at the external surface of zeolite is diffusion-controlled one. According to Laviron's procedure,[21] the relevant kinetic parameters of the Mn^{2+}-zeolite/PDDA electrode reaction, *i.e.*, the rate constant of the electrochemical process (k_s) and electron transfer coefficient (α_c, α_a), were estimated as: $k_s = 2.3 \pm 0.4$ s^{-1}, $\alpha_c = 0.54 \pm 0.03$, and $\alpha_a = 0.56 \pm 0.04$.

Analytical performance of $O_2^{\bullet -}$ biosensor

As demonstrated above, Mn^{2+}-ZSM/PDDA electrode, in which Mn^{2+} was stably confined in the zeolite, can be employed for construction of third-generation $O_2^{\bullet -}$ biosensor because of the biomimetic catalytic activity of Mn^{2+} toward $O_2^{\bullet -}$, as well as the facilitated electron transfer of Mn^{2+} immobilized in the zeolite. As shown in Fig. 4, both anodic and cathodic peak currents corresponding to the redox reaction of Mn^{2+} clearly increased with the addition of $O_2^{\bullet -}$. The observed increases in the anodic and cathodic peak currents could be ascribed to the oxidation and reduction of $O_2^{\bullet -}$, respectively. As reported previously,[18] during the reaction of $O_2^{\bullet -}$ by $Mn_3(PO_4)_2$, two $O_2^{\bullet -}$ ions are converted to one O_2 molecule and one H_2O_2 molecule. Proposed

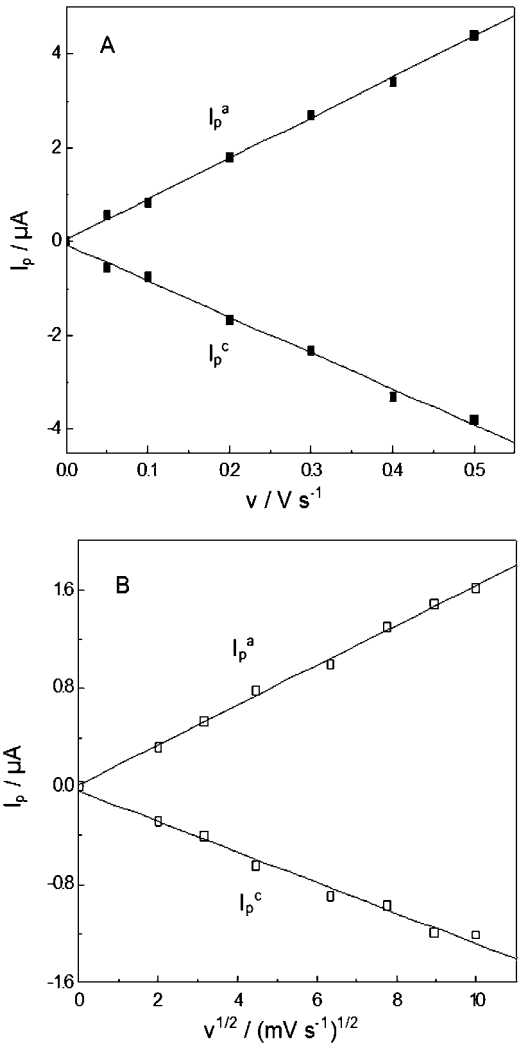

Fig. 3 Relationship between anodic and cathodic peak currents and scan rates for Mn^{2+}-ZSM/PDDA electrode (A) and Mn^{2+}/ZSM/PDDA electrode (B) in 50 mM K_3PO_4 solution (pH 7.0).

electron transfer pathway in $O_2^{\bullet -}$ dismutation is illustrated in Scheme 1. Namely, one $O_2^{\bullet -}$ oxidizes the Mn^{2+} to generate MnO_2^+ and H_2O_2, while another $O_2^{\bullet -}$ reduces the MnO_2^+ to produce Mn^{2+} and O_2. We can consider these two redox process separately by fabricating two electrodes on which each reaction occurs separately. In the anodic process (Scheme 1(A)), the redox reaction between $O_2^{\bullet -}$ and MnO_2^+ takes place to produce O_2 and Mn^{2+}. The generated Mn^{2+} can be reoxidized at the electrode. On the other hand, in the cathodic process (Scheme 1(B)), $O_2^{\bullet -}$ oxidizes the Mn^{2+} to generate MnO_2^+ and H_2O_2. The generated MnO_2^+ can be reduced at the electrode. Thus, by measuring the oxidation or reduction current at the Mn^{2+}-zeolite/PDDA electrode in the presence of $O_2^{\bullet -}$, we can detect $O_2^{\bullet -}$, that is, the present Mn^{2+}-zeolite/PDDA electrode, which is based on direct electron transfer of Mn^{2+}, combined with the specificity and selectivity of $Mn_3(PO_4)_2$ toward $O_2^{\bullet -}$, provides a platform for determination of $O_2^{\bullet -}$ with high analytical performance.

Fig. 5A depicts amperometric responses obtained at Mn^{2+}-zeolite/PDDA surface with the successive addition of $O_2^{\bullet -}$ at the applied potential of 0.6 V or −0.1 V. Both anodic and cathodic

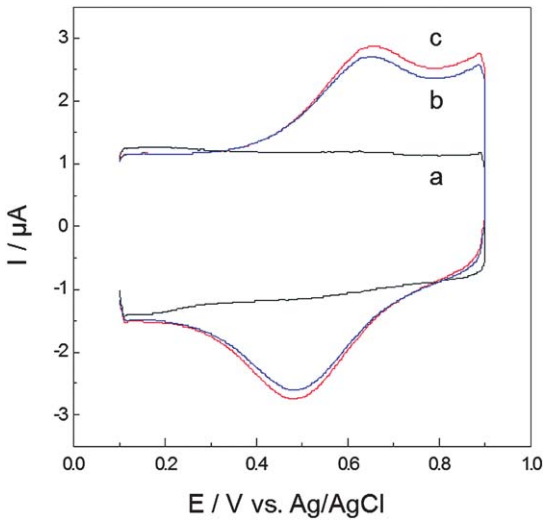

Fig. 4 CVs obtained at (a) ZSM/PDDA electrode and (b and c) Mn^{2+}-ZSM/PDDA electrode in 50 mM K_3PO_4 solution (pH 7.0) in the absence (b) and presence (c) of 100 μM $O_2^{\bullet -}$. Potential scan rate: 100 mV s^{-1}.

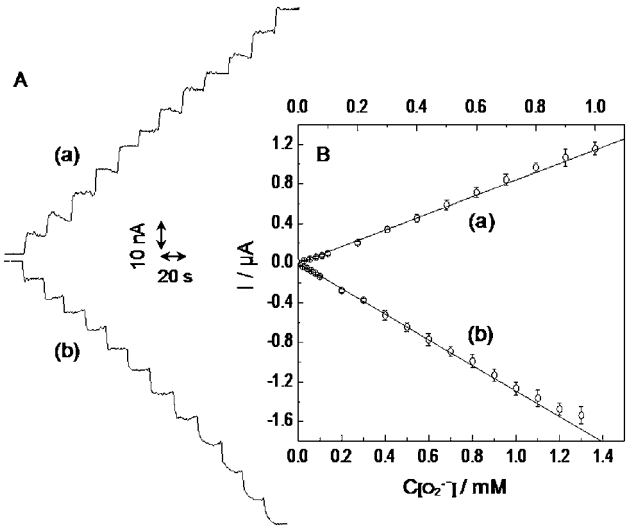

Fig. 5 (A) Typical amperometric responses of Mn^{2+}-ZSM/PDDA electrode to successive addition of 10 μM $O_2^{\bullet -}$ at the applied potentials of +600 mV (a) and −100 mV (b) in 50 mM K_3PO_4 (pH 7.0). (B) Calibration plots of anodic (a) and cathodic (b) steady-state currents against concentration of $O_2^{\bullet -}$.

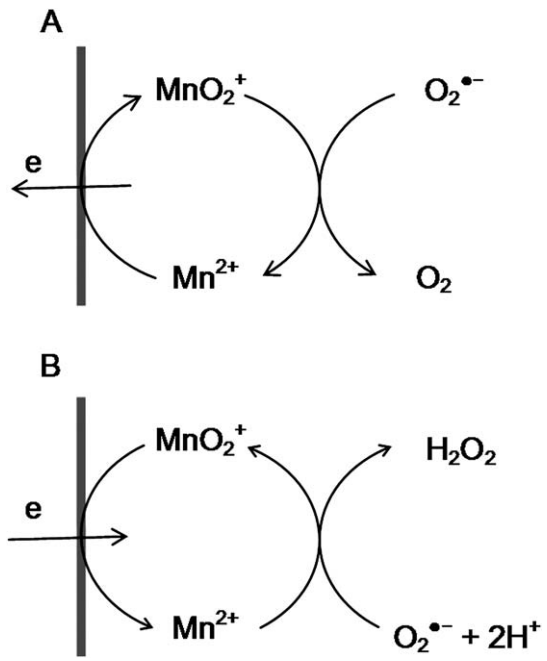

Scheme 1 Schematic illustration of $O_2^{\bullet -}$ dismutation catalyzed by Mn^{2+}/MnO_2^+ confined into the zeolite electrode surface. (A) The oxidation process and (B) the reduction process.

currents increased stepwise with the increasing concentration of $O_2^{\bullet -}$, and typical responses are proportional to the concentration of $O_2^{\bullet -}$ in the range of 5×10^{-7} to 1.2×10^{-3} M at either 0.6 V or −0.1 V, as plotted in Fig. 5B. The wide dynamic linear range meets the requirements of $O_2^{\bullet -}$ detection from nanomolar level to millimolar grade for tracking the role that $O_2^{\bullet -}$ plays in physiological and pathological processes, because under normal physiological conditions, $O_2^{\bullet -}$ undergoes disproportionation by enzymatic reactions, resulting in a rather low physiological concentration (~10^{-7} M), however, increases in the activity of $O_2^{\bullet -}$ (10^{-4}–10^{-3} M) occur in response to traumatic brain injury ischemia-reperfusion, hypoxia, and environmental stresses.[22–24] The detection limit was calculated by three times of instrument noise ($S/N = 3$) to be as low as 0.37 μM, and the response time was estimated to be within 5 s.

The interferences from ROS including H_2O_2, $OH^{\bullet}$, $ONOO^-$, $^1O_2$, $ROO^{\bullet}$, and other biological substances, such as Na^+, Ca^{2+}, K^+, Mg^{2+}, Zn^{2+}, Fe^{3+}, dopamine (DA), ascorbic acid (AA), uric acid (UA), and cysteine (Cys), as well as O_2 which exists extensively in biological system, were investigated. At the applied potential of +0.6 V, 13.15%, 10.15%, 28.43%, and 2.87% current responses generated from $ONOO^-$, 10 μM AA, 5 μM DA, and 5 μM Cys were obtained relative to 10 μM $O_2^{\bullet -}$. Other interferences showed negligible responses. On the other hand, at the potential of −0.1 V, 6.51%, 9.83%, 7.28%, and 6.72% cathodic current was observed from $OH^{\bullet}$, $ONOO^-$, $^1O_2$, 10 μM AA, while other interferences were negligible (<1%), indicating the good selectivity of the present biosensor for $O_2^{\bullet -}$.

For the stability test, the response current for $O_2^{\bullet -}$ was recorded three times daily at Mn^{2+}-ZSM/PDDA electrode and the current responses were found to be constant over four months, which are much longer than those obtained for enzyme-based $O_2^{\bullet -}$ biosensors.[14,25] The further reproducibility experiment was performed by testing the response current for $O_2^{\bullet -}$ by using five as-prepared Mn^{2+}-ZSM/PDDA electrodes respectively and the response variation was less than 4.2%.

In situ determination of $O_2^{\bullet -}$ released from living cells

As demonstrated above, the present $O_2^{\bullet -}$ biosensor based on Mn^{2+}-zeolite/PDDA surface exhibits good selectivity, broad linear range, low detection limit, and quick response. More importantly, Mn^{2+}-zeolite/PDDA surface shows relatively long-term stability and high reproducibility. These properties provide a platform to adhere cells directly onto the electrode surface, and subsequently establish a reliable and durable approach for *in situ*

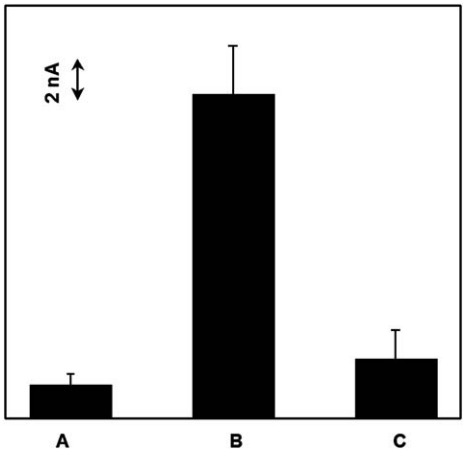

Fig. 6 Electrochemical responses of Mn^{2+}-ZSM/PDDA electrode toward Hela cells at an applied potential of −0.1 V in the absence (A) and presence (B) of 10 mM zymosan (C) with the addition of 300 U mL^{-1} SOD solution.

monitoring of $O_2^{\bullet -}$ released from living cells with high analytical performance. Fig. 6 depicts electrochemical responses obtained at the Mn^{2+}-zeolite/PDDA surface and toward Hela cells adhered on the electrode surface at the applied potential of −0.1 V in the absence (A) and presence (B) of zymosan, which was reported to generate $O_2^{\bullet -}$ from cells.[26] A much higher increased cathodic current was observed after the addition of zymosan. According to the calibration plots shown in Fig. 5B, the concentration of $O_2^{\bullet -}$ released from about 2.5×10^6 Hela cells (Fig. 6B) was estimated to $\sim 1.1 \times 10^{-5}$ M. Interestingly, after injection of 10 μL 300 U mL^{-1} SOD solution, a selective scavenger of $O_2^{\bullet -}$, to the electrode surface, the increased current decreased rapidly and went down to the almost background value in 5 s (C). Thus, we can conclude that the generated increase of cathodic current at the Mn^{2+}-zeolite/PDDA electrode adhered with Hela cells is ascribed to the biomimetic catalytic reduction of $O_2^{\bullet -}$ released from living cells, which is effectively mediated by the Mn^{2+} confined into the zeolite.

Conclusions

A selective and sensitive approach for real-time determination of $O_2^{\bullet -}$ has been developed based on a biomimetic superoxide dismutase (SOD)—$Mn_2(PO_4)_3$, which is confined into the zeolite and further coated by PDDA on the electrode surface. Quasi-reversible electrochemical reaction of Mn^{2+} has been realized at zeolite surface with an electron transfer rate constant of 2.3 ± 0.4 s^{-1}. The facilitated electron transfer of Mn^{2+}, combined with the biomimetic catalytic activity of $Mn_2(PO_4)_3$ has provided a platform for determination of $O_2^{\bullet -}$ with high selectivity, low detection limit, and wide dynamic linear range. Meanwhile, the present Mn^{2+}-zeolite/PDDA electrode has shown long-term stability and biocompatibility. The remarkable analytical performance of the biosensor, as well as the inherent characteristic of biomimetic surface, has established a reliable and durable way to real-time monitoring of cellular $O_2^{\bullet -}$. This investigation not only opens up a new way to real-time determination of cellular $O_2^{\bullet -}$ which may be related to physiological and pathological processes, but also provides a methodology to construct the third-generation biosensors with long-term stability and durability based on the biomimetic enzymes.

Acknowledgements

This work is financially supported by National Natural Science Foundation of China (20975075), the Program for New Century Excellent Talents in University (NCET-06-0380) from State Education Ministry, China, and Nanometer Science Foundation of Shanghai (0952nm04900). Tongji University is also greatly acknowledged.

Notes and references

1 F. Auchere and F. Rusnak, *JBIC, J. Biol. Inorg. Chem.*, 2002, **7**, 664–667.
2 R. T. Dean, S. Fu, R. Stocker and M. J. Davies, *Biochem. J.*, 1997, **324**, 1–18.
3 B. Halliwell and J. M. C. Gutteridge, *Biochem. J.*, 1984, **219**, 1–14.
4 W. Wang, H. Fang, L. Groom, A. Cheng, W. Zhang, J. Liu, X. Wang, K. Li, P. Han, M. Zheng, J. Yin, W. Wang, M. Mattson, J. Kao, E. Lakatta, S. Sheu, K. Ouyang, J. Chen, R. Dirksen and H. Cheng, *Cell*, 2008, **134**, 279–290.
5 P. Kovacic and J. D. Jacintho, *Curr. Med. Chem.*, 2001, **8**, 773–796.
6 J. L. Zweier, J. H. Flaherty and M. L. Weisfeldt, *Proc. Natl. Acad. Sci. U. S. A.*, 1987, **84**, 1404–1407.
7 Y. Ohara, T. E. Peterson and D. G. Harrison, *J. Clin. Invest.*, 1993, **91**, 2546–2551.
8 T. Ohyashiki, M. Nunomura and T. Katoh, *Biochim. Biophys. Acta*, 1999, **1421**, 131–139.
9 J. Vasquez-Vivar, N. Hogg, K. A. Pritchard and B. Kalyanaraman, *FEBS Lett.*, 1997, **403**, 127–130.
10 S. Mesaros, Z. Vankova, S. Grunfeld, A. Mesarosova and T. Malinski, *Anal. Chim. Acta*, 1998, **358**, 27–32.
11 C. J. McNeil, K. R. Greenough, P. A. Weeks and C. H. Self, *Free Radical Res. Commun.*, 1992, **17**, 399–401.
12 V. Lvovich and A. Scheeline, *Anal. Chem.*, 1997, **69**, 454–461.
13 B. Ge and F. Lisdat, *Anal. Chim. Acta*, 2002, **454**, 53–64.
14 Z. Deng, Q. Rui, X. Yin, H. Liu and Y. Tian, *Anal. Chem.*, 2008, **80**, 5839–5846.
15 Y. Tian, L. Mao, T. Okajima and T. Ohsaka, *Anal. Chem.*, 2002, **74**, 2428–2436.
16 Y. Tian, L. Mao, T. Okajima and T. Ohsaka, *Anal. Chem.*, 2004, **76**, 4162–4168.
17 Y. Tian, L. Mao, T. Okajima and T. Ohsaka, *Biosens. Bioelectron.*, 2005, **21**, 557–564.
18 Y. Luo, Y. Tian and Q. Rui, *Chem. Commun.*, 2009, 3014–3016.
19 J. A. Martens, I. Balakrishnan, P. J. Grobetand and P. A. Jocabs, *Stud. Surf. Sci. Catal.*, 1991, **69**, 135–143.
20 Z. Zhu, Q. Chen, Z. Xie, W. Yang, D. Kong and C. Li, *J. Mol. Catal. A: Chem.*, 2006, **248**, 152–158.
21 E. Laviron, *J. Electroanal. Chem.*, 1979, **101**, 19–28.
22 R. A. Floyd, *FASEB J.*, 1990, **4**, 2587–2597.
23 E. D. Hall and J. M. Braughler, *Free Radicals Biol. Med.*, 1989, **6**, 303–313.
24 H. A. Kontos and E. P. Wei, *J. Neurosurg.*, 1986, **64**, 803–807.
25 H. Liu, Y. Tian and P. Xia, *Langmuir*, 2008, **24**, 6359–6366.
26 Q. Lin, L. Jin, Z. Cao, Y. Lu, H. Xue and Y. Xu, *Phytother. Res.*, 2008, **22**, 740–745.

